Ind J Eng Mgt Sci. 2025(Oct-Dec);1(1):1-11

Indian Journal of Engineering, Management and Technology

https://doi.org/XX.XXXX/ijems.XXXX

Research Article

Colossal Magnetoresistance in Manganites: An Overview and Field-Dependent Transport Study of $La_{3/5}Sr_{2/5}MnO_3$ Perovskite

Vijaylakshmi Dayal[a]

[a]*Department of Physics, Maharaja Institute of Technology Mysore, Mandya, Karnataka 571477, India*
Email: drvldayal@gmail.com; drvldayal@mitmysore.in

Received: 16-05-2025, *Accepted*: 20-09-2025, *Published*: 28-09-2025

Abstract

Transition metal oxides with perovskite structures have attracted considerable attention owing to their wide-ranging electrical and magnetic properties, positioning them as promising materials for next-generation electronic and spintronic devices. Among these, manganite-based compounds exhibiting colossal magnetoresistance (CMR) have been extensively studied for their potential in magnetic sensors, data storage, and related technologies. In this context, the present study focuses on the structural, electrical, and magneto-transport properties of $La_{3/5}Sr_{2/5}MnO_3$ perovskite, a composition well known for its pronounced CMR behavior. X-ray diffraction analysis confirms the formation of a single-phase perovskite structure with high crystallinity. Temperature-dependent resistivity (ρ–T) measurements were performed under magnetic fields of 0 T, 4 T, and 8 T. The material exhibits a distinct metal-insulator transition (T_{MI}) at 230.56 K in the absence of a magnetic field. With the application of magnetic fields, the T_{MI} shifts to higher temperatures, which is attributed to enhanced carrier delocalization mediated by the double exchange mechanism. A marked reduction in resistivity is observed at higher magnetic fields, resulting from suppressed spin disorder and diminished inelastic electron scattering. The conduction mechanism is further analyzed using small polaron hopping and variable range hopping models, suggesting a temperature-dependent transport regime. Isothermal magnetoresistance (MR%) measurements at 5 K over a 0–8 T range indicate significant negative MR, which is interpreted using the spin-polarized tunneling model, emphasizing the role of grain boundary effects in charge transport. The compound's notable CMR response positions it as a promising material for future applications in magnetic sensors and spintronic technologies.

Keywords: Manganites and its characteristics, Electrical Resistivity, Phase transition, Magnetoresistivity

1. Introduction

Transition metal oxides of the perovskite structure with compositions and their layered structure relatives $A_{n+1}B_nO_{1+3n}$ (n = 1, 2, 3) exhibit a variety of interesting electrical and magnetic properties. Such compounds can be of numerous categories, depending on their origin and application. The versatility of perovskite oxides for electronic applications is demonstrated by the fact that these materials exhibit a wide range of conductivity, ranging from a highly conducting metallic state to an insulating state [1]. The discovery of colossal magnetoresistance (CMR) properties in manganite perovskites has offered very promising field for the investigation

of new materials with specific properties susceptible to be involved in device applications [2]. These metal oxides are strategically important and expected to have widespread industrial applications, including fuel cells, magnetic sensors, electronic devices, microwave components, data storage and magnetic recording devices, chemical and gas sensors, catalysts, and spin devices [1,3]. The discovery of these CMR materials raised expectations of a new generation of magnetic devices and sensors, such as magnetic data storage and magnetic read heads. The belonging of CMR materials to the perovskite family is an additional advantage. It allows for making smart devices and fabricating epitaxial hetero-structures with alternating layers that possess identical crystalline and different functional properties [4].

Magnetoresistance (MR) is the relative change in the electrical resistance or resistivity of a material produced by the application of a magnetic field. It is generally defined by,

$$\mathrm{MR\%} = \left(\frac{\rho(0)-\rho(\mathrm{H})}{\rho(0)}\right) \times 100 \ldots\ldots\ldots\ldots\ldots\ldots (1)$$

Here ρ(0) and ρ(H) resistivities at a given temperature in the applied (H) and zero (0) magnetic field, respectively. MR, in general, can be positive or negative depending on the increase or decrease in resistivity, respectively [2,4]. Large magnetoresistance, referred to as giant magnetoresistance (GMR), has been observed in layered and granular magnetic materials (e.g., polycrystalline sputtered Fe/Cr multilayers [5], Co/Cu and related multilayers [5,6]. This phenomenon is also been observed in inhomogeneous granular (clusters and alloys) systems predominately comprised of Fe, Co, Ni, and their various alloys in Cu, Ag, and Au matrices [7–9], in nickel-contacted carbon nanotubes [10], and Cu-Co-Ni alloy films [11]. Among the several discussed materials, manganites have been studied for many years [12,13]. The burst of activity was motivated by the breakthrough of spectacularly large MR in mixed valence ABO_3 [2,3,14]. The above class of material was epitomized by colossal magnetoresistance (CMR), to distinguish it from the GMR. Where A and B are trivalent and divalent elements, respectively. These materials show a large magnetoresistance effect and, in general, are known as colossal magnetoresistive (CMR) materials. The CMR parent compounds $AMnO_3$ and $BMnO_3$ (A is a trivalent and B is a divalent element) form an ideal cubic perovskite structure. It consists of a three-dimensional network of a vertex sharing MnO_6 octahedral and interstitial "A/B" cations [15–17]. The ideal cubic structure is distorted by cation substitution and/or oxygen off-stochiometry. It is mainly due to cation size mismatch and the Jahn-Teller effect, the electron instability. The ideal cubic structure is modified into a lower symmetry structure, such as orthorhombic, rhombohedral, etc., due to the following three mechanisms [18][19], Viz (i) cooperative tilting of the octahedra, (ii) displacement of the cations, and (iii) distortions of the octahedra. The tilting of the octahedra is the most relevant in deciding the overall space group symmetry of the particular manganite perovskite. Further, in order to fill the empty space due to size mismatch in 'A/B'site octahedral rotate cooperatively. This distortion is characterized by the Goldsmith tolerance factor[20];

$$t = {d_{\left(\frac{A}{B}\right)-O}}\Big/{d_{(Mn)-O}} \ldots\ldots\ldots\ldots\ldots\ldots\ldots\ldots (2)$$

where $d_{(A/B)-O}$ and $d_{(Mn)-O}$ are the average or cation-oxygen and distances, respectively. In the case of cubic perovskite $t = 1$, the stable perovskite structure is found for values in the range of 0.8 to about 1.1 [21]. Perovskite containing small cations leads to $t < 1$, while large cations give rise to $t > 1$. For, $t \sim 1$, the $\bar{R}3c$ space group is formed with rhombohedral symmetry.

In 1954, Volger [21] reported negative MR with a peak near the Curie temperature in $La_{0.8}Sr_{0.2}MnO_3$. Soon after, Volger, Wollen, and Koehler [22] carried out extensive neutron diffraction studies to characterize and draw the first magnetic structure of $La_{1-x}Ca_xMnO_3$ in the entire composition range. They also concluded that, in addition to the ferromagnetic phase, other interesting antiferromagnetic phases are also present in manganites. Further progress came somewhat later with the reported negative MR in single crystals of $(La,Pb)MnO_3$, with a Curie temperature well above room temperature [17,22,23]. Jirak et al. [24] and Pollert et al. [24] observed a charge-ordered phase in $(Pr,Ca)MnO_3$ by X-ray and neutron diffraction techniques. They observed charge-ordered phases, which are different from the ferromagnetic phases of other manganites. The divalent doped perovskite manganite $La_{1-x}A_xMnO_3$ (A = Ca, Ba, and Sr) has been thoroughly investigated due to its ferromagnetic behavior at room temperature for a few compositions, both from the fundamental and

the applied perspective [25,26]. Mixed valent Mn^{3+} and Mn^{4+} ions are developed at the Mn-site when trivalent rare-earth (La^{3+}) ions in $LaMnO_3$ are replaced by the divalent alkaline-earth elements (Ca^{2+}, Ba^{2+}, Sr^{2+}, etc.). Depending on the ratio of the Mn^{3+} and Mn^{4+} ions, the double exchange (DE) [27,28] and super-exchange (SE) interactions occur [29]. The competition between the DE and SE interactions has been correlated with understanding the significant enhancement/decrement in electrical conductivity and magnetization behavior [30,31]. The correlation between ferromagnetism and metallic conductivity in manganites can be ascribed using Zener double exchange interaction [32] to an indirect coupling between the "incomplete d-shells" of the Mn^{3+} and Mn^{4+} and via the "conducting electron" of oxygen. In addition to the indirect exchange interactions, there exists a superexchange mechanism between neighboring t_{2g} orbitals, which is typically antiferromagnetic. The electrical conductivity in these materials arises from the mixed valence states of manganese ions. Zener proposed a mechanism, now known as double exchange (DE), to explain this behavior, wherein an electron is transferred from one Mn ion to a neighboring Mn ion via an intermediate oxygen ion. This involves two simultaneous processes: the electron first hops from the Mn^{3+} ion to the oxygen 2p orbital, followed by a transfer from the oxygen to a neighboring Mn^{4+} ion. The basic idea of the DE mechanism is that two configurations, Mn^{3+}- O^{2-}-Mn^{4+} and Mn^{4+}- O^{2-}-Mn^{3+}, are energetically degenerate. The configurations are written in the form;

$\psi_1 = Mn^{3+} - O - Mn^{4+}$, and

$\psi_2 = Mn^{4+} - O - Mn^{3+}$ .....(3)

These configurations differ only in the direction of electron (or hole) hopping between Mn ions via the intermediate oxygen (O) ion, but both contribute equally to the delocalization of charge carriers. Thus, the configurations degenerate in energy, leading to a delocalization of the hole on the Mn^{4+} site or electron on the Mn^{3+} site. Zener pointed out that the degeneracy of these two corresponding wave functions makes this process fundamentally different from conventional super-exchange, occurring between similar ions, like Mn^{3+} -Mn^{3+} or Mn^{4+} -Mn^{4+}. The coupling of these degenerate states lifts the degeneracy and allows the system to resonate between two configurations (ψ_1 and ψ_2). When the core spins are aligned parallel, the resonance promotes both metallic conductivity and ferromagnetism. Zener estimated the splitting to be given by the ferromagnetic transition temperature T_c and, based on Einstien's relation and the diffusion constant of a hole located at a Mn^{4+} site, predicted the electrical conductivity, σ at any particular temperature, T, should take the form:

$$\sigma \approx \frac{x.e^2}{a.h} \cdot \frac{T_c}{T} \quad \text{..... (4)}$$

where, x =concentration of Mn^{4+} ions, e=electronic charge, h= Planck's constant and a= lattice parameter or Mn-Mn distance. Zener's model was based on the assumption that the manganites are uniform and homogenous without any form of coexisting clusters of competitive phases. Anderson and Hasegawa (1955) [33] modified Zener's argument, treating the core spin of each Mn ion classically and the mobile electron quantum mechanically, demonstrating that effective electron hopping depends on the alignment of neighboring Mn core spins. Further refinements and quantum mechanical treatments were provided by Goodenough [25], de Gennes, Kubo, and Ohata, enlarging the theoretical understanding of phase transitions and transport mechanisms [1].

The divalent-doped manganite $(La,Sr)MnO_3$ is a compound with an ABO_3-type perovskite structure. In this structure, the A-site cations (La^{3+}/Sr^{2+}) occupy the corners of the unit cell, the B-site cations (Mn^{3+}/Mn^{4+}) are located at the body center, and the (O^{2-}) ions are positioned at the face centers, forming a BO_6 octahedral network. The compound exhibits a complex electronic phase diagram that varies with Sr^{2+} doping levels, influencing its electronic and magnetic characteristics [1,3,15]. At the two extremes of doping, x = 0 ($LaMnO_3$) and x=1 ($SrMnO_3$), the system demonstrates insulating A-type and G-type antiferromagnetic (AFM) behaviors, respectively. For doping levels up to $x \leq 0.18$, the compound shows charge-ordered A-type AFM behavior, attributed to long-range Jahn-Teller distortions. As the Sr content increases to the range of $0.18 < x < 0.40$, these distortions are gradually suppressed. Initially, the system transitions to a ferromagnetic (FM) insulating phase (for $x < 0.20$), and eventually to a ferromagnetic metallic phase. Beyond $x > 0.40$, the material reverts to AFM ordering (C-type and CE-type), accompanied by insulating behavior. The doping range of $0.30 \leq x \leq 0.40$ is particularly significant, as it supports a robust FM metallic

phase with a high Curie temperature (T_C ~ 370 K) and complete spin polarization. This makes it highly attractive for room-temperature spintronic applications. Further, the physical properties of (La,Sr)MnO_3 are strongly influenced by the synthesis method, especially when preparing high-quality ceramics [34]. Ceramics made of fine particles with significant grain boundary effects at low temperatures may exhibit enhanced properties. Materials with smaller grain sizes are of particular interest due to the increased structural and magnetic disorder at grain boundaries, which can lead to novel electronic and magnetic phenomena [35]. Various synthesis methods have been employed to produce these manganites with controlled particle sizes [34,36,37].

In light of this, the present work focuses on the structural, electrical conductivity, and magneto-transport properties of $La_{3/5}Sr_{2/5}MnO_3$ perovskite, a composition known to exhibit pronounced CMR effects. Field-dependent resistivity measurements have been performed to study the transport behavior and magnetoresistance (MR). The following sections present the synthesis procedure, structural characterization, and comprehensive analysis of electrical and magneto-transport data, providing insights into the fundamental mechanisms governing CMR in this compound.

2. Experimental

The manganite Perovskite $La_{3/5}Sr_{2/5}MnO_3$ in nanocrystallite size has been synthesized by the conventional citric-nitrate gel combustion method [30]. High-purity precursor materials—La_2O_3 (99.99%), $SrCO_3$ (99.9%), and MnO_2 (99.9%)—procured from Sigma Aldrich & Co., were accurately weighed in stoichiometric proportions. To facilitate the dissolution of La_2O_3, $SrCO_3$, and MnO_2 were dissolved in diluted nitric acid, which yielded a light-yellow solution. The nitric acid was diluted using nanopure deionized water. The solutions were mixed and continuously stirred and heated at 80 °C to obtain a clear solution. A measured amount of. Subsequently, citric acid was added in a 3:1 molar ratio (citric acid to metal nitrates) to promote the redox reaction, where citric acid acted as the fuel/reductant and nitric acid as the oxidizer. The resulting mixture was maintained at 80 °C under constant stirring until most of the water content evaporated and a gel-like precursor formed. This gel was then subjected to heating at 400 °C for 2 hours to produce a dry powder, followed by multiple grindings. The powder was calcined sequentially at 500 °C and 600 °C for 8 hours with intermittent grinding steps to ensure homogeneity. Finally, the sample was sintered at 700 °C for 10 hours. Phase analysis of the synthesized sample was performed using X-ray diffraction (XRD). DC electrical resistivity and magnetoresistance as functions of temperature and magnetic field were measured using the standard four-probe method down to 5 K. For magneto-transport measurements, the magnetic field was applied parallel to the current direction using an Oxford Spectromag 8T superconducting magnet at the UGC-DAE Consortium for Scientific Research, Indore.

3. Results and Discussion

The powder X-ray diffraction pattern (PXRD) of the nanomaterial is shown in Fig.1. The XRD diffractogram could be indexed to $R\bar{3}c$ space group having rhombohedral perovskite structure without any impurity phase present. The XRD patterns were analyzed and refined using the Rietveld refinement technique [38][39] through Fullprof Software [40], exhibiting strong correspondence with the calculated patterns with the reliability factor ($\chi^2 = 2.2$), and the refined lattice parameters have been calculated to be a=5.473 Å and c=13.340 Å, and the cell volume is found to be 399.74 $Å^3$. The average crystallite size can be calculated using well well-known Scherrer formula [41] given as,

$$D = \frac{K\lambda}{\beta cos\theta} \quad \ldots\ldots\ldots\ldots\ldots\ldots\ldots\ldots\ldots (5)$$

Where λ is the X-ray wavelength in nanometers (nm), β is the full-width half maximum (FWHM) obtained from Pseudo-Voigt fitting to the XRD pattern, and $K = 0.92$ is a constant related to grain shape. The average crystallite size (D) is found to be 16.39 nm, suggesting that the sample is formed in a nanocrystalline size.

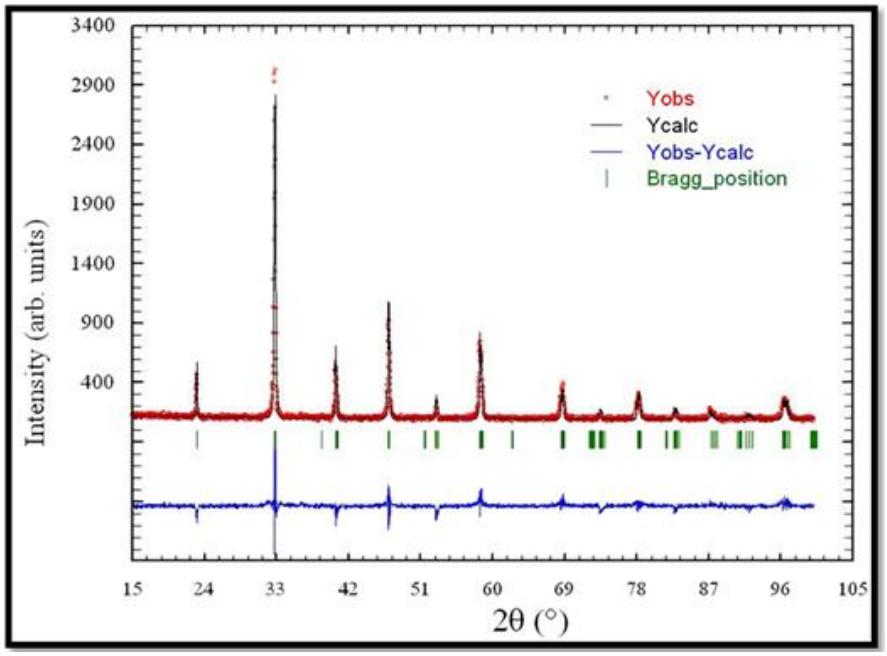

Fig. 1: The X-ray diffraction pattern of the powdered sample at room temperature using Cu-K_α radiation is shown.

In order to quantify the size mismatch of the A and B site cations, we have calculated the Goldschmidt tolerance factor 'τ', as discussed in the introduction section (eq.2). The value of 'τ' is calculated to be 0.910. The ideal $\tau < 1$ in the above-mentioned sample is due to the cooperative rotation of MnO_6 octahedra about a specific cubic axis, giving a slight structural distortion ($c/a > 1.41$). This type of rotation changes the Mn-O-Mn bond angle from 180°, which indeed affects the DE interactions and induces criticality in lattice arrangements.

Fig. 2 (a) shows an electrical resistivity (ρ) vs. temperature (T) plot measured under different magnetic fields of 0, 4, and 8T. The sample exhibits ferromagnetic metallic to paramagnetic insulating (MI) phase transition at a temperature (T_{MI}) as summarized in Table 1. Upon applying the magnetic field, the resistivity decreases significantly and T_{MI} shifts to the higher temperature side. This behavior is attributed to the magnetic-field-induced delocalization of charge carriers. The increase in resistivity observed at low temperatures is primarily due to carrier localization caused by enhanced electron–phonon interactions and grain boundary scattering, discussed in detail later in Figs. 4 and 5. The upward shift in T_{MI} with increasing magnetic field is likely driven by the field-induced alignment of Mn spins, which strengthens the double exchange (DE) interaction and suppresses spin-disorder scattering, thereby enhancing carrier mobility[32].

This interpretation is further supported by the magnetoresistance (MR) behavior with temperature at magnetic fields of 4 and 8T, shown in Fig. 2(b). The MR% has been calculated using Eq. 1. The MR is negative throughout the temperature range and reaches values of approximately -32% at low temperatures (~10 K) under 4 T, and about -41% under 8 T. The pronounced negative MR highlights the suppression of spin disorder and improved electronic transport under magnetic fields, confirming strong coupling between charge carriers and spin ordering.

For understanding the resistivity behavior in the metallic region ($T < T_{MI}$), the resistivity vs. temperature has been analyzed with the empirical equation [42,43];

$$\rho_{FM}(T) = \rho_0 + \rho_1 T^n \quad \text{.....(6)}$$

Here ρ_0 is the residual resistivity independent of temperature due to scattering by impurities, defects, grain boundaries, and domain walls. The ρ_1 in the above equation is ascribed to the scattering of electron-electron or electron–magnon scattering. The fitting of the resistivity plot at low temperatures ($T < T_{MI}$) using Eq. 6 shows the reasonable values of $n = 1.4$, which is around 2 with the varying magnetic field (0T, 4T, and 8T), suggesting the electron-electron and electron magnon interaction. The best-fit parameters obtained from the fitting with Eq. 6 are shown in Table 1.

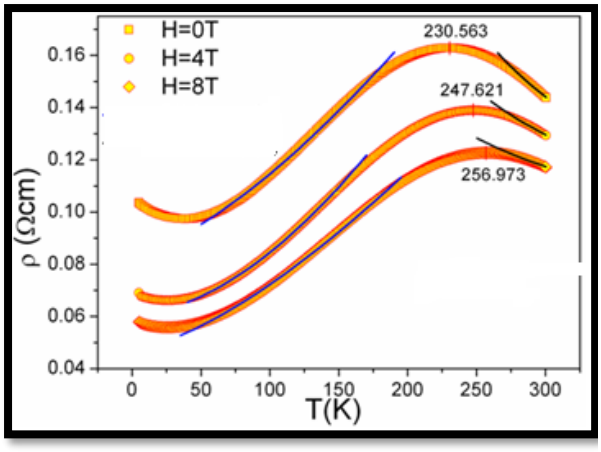

Fig 2: Resistivity (ρ) vs. temperature (T) plot of the sample at 0, 4, and 8T magnetic field. The fitted line shows fitting to the empirical model for $T<T_{MI}$ and the variable range hopping model for $T>T_{MI}$.

The electrical conduction mechanism in the insulating region of $\rho(T)$ curve $(T > T_{MI})$ in the perovskite manganite is explored in terms of Variable range hopping (VRH), described by;

$$\rho_{PM}(T) = \rho_{oh} exp[\left(\frac{T_0}{T}\right)^q],\ 0 < q < 1 \ldots..(7)$$

here ρ_{oh} is a coefficient that weakly depends on temperature. The values of $q = \frac{1}{2}\ and \frac{1}{4}$, are obtained due to Shklovskii-Efros (SE-VRH) and Mott's VRH mechanisms, respectively. The T_0 is the characteristic VRH temperature as given by [44].

$$T_0 = 18/(\xi^r K_B N(E_F)) \ldots\ldots\ldots\ldots\ldots\ldots\ldots\ (8)$$

The parameter 'ξ' represents the localization length of the trapped charge carriers, while the exponent 'r' typically assumes values of 2 and 3, corresponding to the small polaron hopping (SE-VRH) and Mott's variable-range hopping (Mott's VRH) mechanisms, respectively. $N(E_F)$ denotes the density of localized states at the Fermi level. The SE-VRH model is found to be suitable for the analysis of high-temperature resistivity data as presented by the fitting of the high-temperature data in the high-temperature region $(T > T_{MI})$ as the nature of fitting with reduced regression (χ^2) factor is less.

Furthermore, the resistivity behavior in the temperature range of 10 to 300 K was analyzed by fitting the data using both the empirical model (eq 6) and the small polaron hopping-based variable-range hopping (SE-VRH) model (eq 7), accounting for contributions from both mechanisms. i.e. $\rho_{FM}(T)$ and $\rho_{PM}(T)$,respectively. The combined equation is written as[30,45–49],

$$\rho_{Whole}(T) = (\rho_0 + \rho_1 T^n) f + (1-f)\rho_{oh} exp\left(\frac{T_0}{T}\right)^{1/2} \ldots\ldots\ldots\ldots\ldots\ldots\ldots\ldots\ldots\ (9)$$

here $f(T) = \{[\exp(T-\frac{T_C^M}{\Delta})] + 1\}^{-1}$ is Boltzmann's distribution function of charge carriers in the metallic state.

The characteristic metal–insulator transition temperature (T_{MI}) is denoted as T_C^M and Δ represents the effective transition width around T_C^M. In Fig. 3, the resistivity data fitted to eq (6) over the temperature range of 75–300 K is shown, where T_C^M and Δ are treated as the only adjustable parameters.

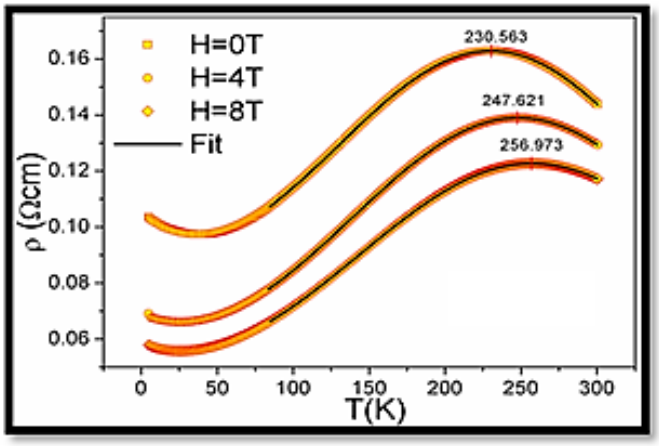

Fig 3: Resistivity (ρ) vs. temperature (T) plot of the sample at 0, 4, and 8T magnetic field, where solid lines show the fitting carried out with the combined $\rho_{FM}(T)$ and $\rho_{PM}(T)$ respectively, using eq. 9.

All other parameters, including like ρ_0, ρ_2, n, ρ_{oh} and T_0 are held constant during the fitting process. Considering the phenomenological nature of the two-phase models given in Eq. (9), the fitting with the experimental data is satisfactory, and the fitted parameters are shown in Table 1.

Additionally, the low-temperature resistivity minimum is observed in large magnetic fields of 4T and 8T.

As there is no magnetic impurity in the sample, no secondary phase is reflected to exist in the XRD pattern. Therefore, the possibility of Kondo scattering can be ruled out. The other factor that can be responsible for this behavior is the low-temperature electron-electron scattering due to coulombic interactions between charge carriers and the weak localization. This nature is possible when the low-temperature resistivity is more than Mott's maximum limit of metallic resistivity of ~ $10^{-3}\Omega$cm. In the studied sample, the electrical resistivity is quite above this governing factor, and hence, the electron-electron elastic scattering is quite formidable. It has already been studied above that the resistivity in the FM metallic region is due to the various electron-phonon and electron-magnon inelastic scattering processes.

This anomalous resistivity in the low-temperature region can be regenerated by adding an electron-electron inelastic scattering term to Eq. 6. The low-temperature resistivity of all the samples has been fitted to this law. The well-fitted low-temperature experimental data of electrical resistivity are shown in Fig. 4.

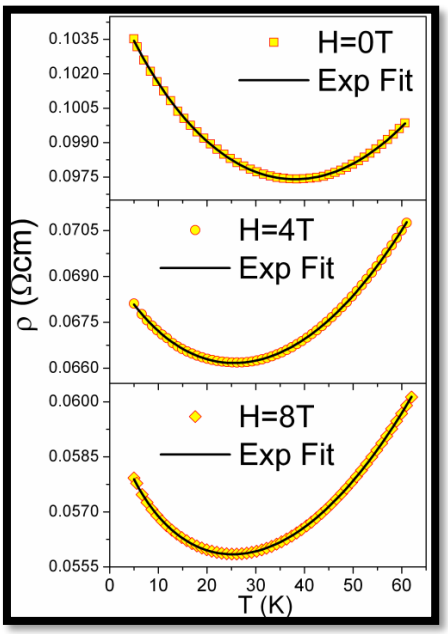

Fig. 4: The low-temperature resistivity data with different magnetic fields. A solid black line represents an experimental fit.

In the temperature range $T \to T_{MI}$ one can expect the critical behavior of $\rho(T)$ to satisfy the scaling law $\rho^{-1}(T) \sim (1 - \frac{T}{T_{MI}})^{v}$. And it follows from Fig. 5 the plots of $ln\left[\frac{1}{\rho(T)} - \frac{1}{\rho(T_{MI})}\right]$ vs. $ln\left(1 - \left(\frac{T}{T_{MI}}\right)\right)$ at $T \to T_{MI}$ are linear.

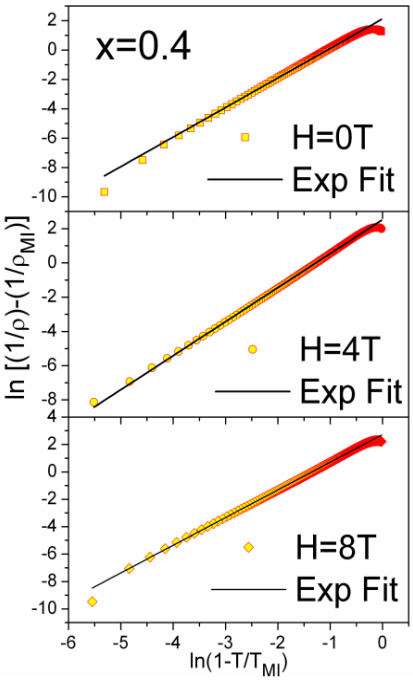

Fig. 5: The low-temperature resistivity data with different magnetic fields. A solid black line represents an experimental fit.

The resistivity data were subjected to linear fitting near the metal–insulator transition temperature ($T \to T_{MI}$), which yielded values of the critical exponent 'v' ranging between 0.9 and 1.02. These values are consistent with theoretical predictions and indicate a gradual change in conduction mechanisms as temperature approaches the transition point [50]. The close similarity in slopes across different magnetic fields suggests a phase separation phenomenon. In this scenario, hole-rich ferromagnetic (FM) metallic regions coexist with the host paramagnetic (PM) insulating matrix. As the system approaches the Curie temperature (T_C), the volume fraction of the FM metallic phase increases, leading to the formation of percolative clusters that enhance conductivity [51].

Fig. 6 displays the magnetoresistance (MR) as a function of the applied magnetic field at various temperatures: 5 K, 100 K, 200 K, and 300 K. A significant drop in resistance is observed at low fields, especially at 5 K. According to the model proposed by Hwang et al. [52], this sharp decrease arises due to the alignment of magnetic domains within the grains, facilitated by the movement of domain walls across grain boundaries.
To explain this behavior more quantitatively, Hwang et al. [52] developed a model based on grain boundary (GB) effects, which is particularly suitable for polycrystalline manganites doped with divalent ions (Sr) at the La site—such as the present $La_{3/5}Sr_{2/5}MnO_3$ system. In this model, the

total resistance *R(H)* under an external magnetic field is considered to have three contributions:

1. R_0 : A field-independent term arising from nonmagnetic lattice defects and static scattering processes.
2. $R_{spt}(H)$: A magnetic field-dependent term attributed to spin-polarized tunneling across grain boundaries.
3. $R_{int}(H)$: Another field-dependent term due to intrinsic magnetic interactions, including spin fluctuations and Zener double exchange mechanisms.

Thus, the total resistance is expressed as:
$R(H) = R_0 + R_{spt}(H) + R_{int}(H)$……(10)
where $R_{spt}(H) = R_{spt}(H = 0)[1 - \int_0^H f(K)\ dk]$, represents the suppression of resistance due to spin-polarized tunneling with increasing field. $R_{int}(H) = -aH - bH^3$, accounts for the intrinsic decrease in resistance due to field-induced spin alignment and magnetic ordering.

To extract and separate the contributions from spin-polarized tunneling and intrinsic effects, magnetoresistance is modeled using the expression:
$MR = -A\int_0^H f(k)dk - JH - KH^3$……(11)
where $f(K) = Ae^{(-BK^3)} + CK^2e^{(-DK^2)}$, the first term, $Ae^{(-BK^3)}$, captures the spin-polarized tunneling effects across GBs, and the second term, $CK^2e^{(-DK^2)}$, represents the intrinsic effects such as Zener double exchange interaction and magnetic spin fluctuations.

By differentiating the MR equation with respect to the magnetic field H, the final expression for fitting becomes [52]:
$\frac{d(MR)}{dH} = Ae^{(-BH^2)} + CH^2e^{(-DH^2)} - J - 3KH^2$…… (12)

The experimental MR data were fitted using this model, and the best-fit parameters were obtained as follows: A=-77.88, B=13.6×10^3, C=4.62, D=0.87, J=4.91, and K=0.01 . This model provides a quantitative method for deconvoluting the total MR response into its fundamental components: spin-polarized intergranular tunneling and intrinsic magnetic interactions. The successful application of this model confirms the coexistence of extrinsic grain boundary effects and intrinsic spin-dependent scattering mechanisms in the magnetotransport behavior of divalent-doped polycrystalline manganites.

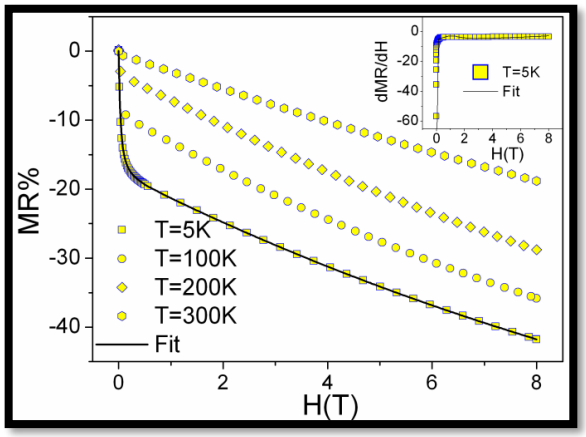

Fig. 6: Magnetoresistance (MR%) as a function of magnetic field measured at various temperatures (5 K, 100 K, 200 K, and 300 K).

The solid lines represent the interpolation fits based on the theoretical model. The inset shows the corresponding curve fitting using the differential expression (Equation 10), highlighting the contributions from spin-polarized tunneling and intrinsic magnetic interactions.

The well-fitted experimental curves indicate that the adopted fitting procedure is both reliable and self-consistent, effectively capturing the underlying magnetotransport mechanisms [52].

TABLE 1. The fitting parameters related to various fittings for the studied samples are presented.

H (T)	ρ_0 (10^{-2} Ωcm)	ρ_1 (10^{-5} Ωcm)	n	ρ_{0h} (10^{-2} Ωcm)	$T_0 \times 10^3$ (K)	T_{MI} (K)	T_C^M(K)	Δ	ν
0	8.42	4.00	1.44	6.18	257.57	230.56	245.21	2.02	1.01
4	6.07	0.68	1.76	6.99	136.91	247.62	263.25	4.03	0.98
8	4.72	3.00	1.44	7.52	71.50	256.97	272.13	5.97	1.08

4. Conclusion

In this study, we successfully synthesized nano-crystalline $La_{3/5}Sr_{2/5}MnO_3$ perovskite via the conventional citric-nitrate gel combustion method. X-ray diffraction analysis confirmed the formation of a pure rhombohedral perovskite structure with an average crystallite size of 16.39 nm. The calculated Goldschmidt tolerance factor (t=0.910) provided insights into the cooperative rotation of MnO_6 octahedra, suggesting a slight structural distortion that

influences the double exchange (DE) interactions and lattice arrangements. Our comprehensive investigation into the electrical resistivity (ρ) as a function of temperature (T) and magnetic field revealed a clear ferromagnetic metallic to paramagnetic insulating phase transition (T_{MI}). The application of an external magnetic field consistently shifted the T_{MI} to higher temperatures, indicative of a delocalization effect. The resistivity data in the metallic region ($T< T_{MI}$) were well-described by an empirical equation suggesting contributions from electron-electron and electron-magnon scattering. For the insulating region ($T>T_{MI}$), the SE-VRH mechanism provided a suitable explanation for the electrical conduction. A combined two-phase model effectively fitted the resistivity behavior across the entire temperature range, underscoring the coexistence of metallic and insulating characteristics. The observed low-temperature resistivity minimum under large magnetic fields was attributed to electron-electron elastic scattering, ruling out Kondo scattering due to the absence of magnetic impurities. Furthermore, analysis of the low-temperature resistivity using a scaling law confirmed the presence of a critical behavior, supporting a phase separation effect where ferromagnetic metallic regions form percolation clusters as the temperature approaches $T_{MI.}$ The magneto-transport properties demonstrated a notable magnetoresistance (MR) effect, with the MR percentage significantly influenced by temperature and magnetic field. The low-field decrease in resistivity at 5 K was explained by a model focusing on the movement of grain boundaries and spin-polarized tunneling, alongside intrinsic contributions from the Zener double exchange mechanism and spin fluctuations. The strong correspondence between the experimental MR data and the fitted model underscores the reliability of this approach in deconvoluting the various contributions to the magnetoresistance.

The findings from this study reinforce the critical role of structural parameters, mixed valency, and the double exchange mechanism in dictating the electrical and magneto-transport properties of $La_{3/5}Sr_{2/5}MnO_3$. The pronounced colossal magnetoresistance observed in this material, coupled with its robust ferromagnetic metallic behavior, highlights its potential for various industrial applications. These include next-generation magnetic sensors, electronic devices, microwave components, data storage, and spin devices, leveraging the inherent advantage of perovskite family materials for fabricating smart epitaxial heterostructures with tunable functional properties. Our work provides fundamental insights that will contribute to the continued exploration and optimization of these strategically important transition metal oxides.

Acknowledgments

VD is thankful to DAE-BRNS (project sanction No: **2011/20/37P/01/BRNS**) and UGC DAE CSR, Indore (sanction No.: **CSR-IC/CRS-89/2014-2015/596**) for financial support. VD gratefully acknowledges Centre director, UGC-DAE Consortium for Scientific Research, Indore for the experimental facilities and extended support. The author is grateful to Dr. Rajeev Rawat and Mr. Sachin Kumar of UGC-DAE Consortium for Scientific Research, Indore for resistivity measurements. The author is indebted to the Maharaja Institute of Technology and Maharaja Research Foundation® (MRF) for necessary support towards the Research.

Conflict of interest: The Author have no conflict of interest.

References

[1] C. Israel, M.J. Calderón, N.D. Mathur, The current spin on manganites The manganites are pseudo-cubic oxides of manganese that show, Mater. Today. 10 (2007) 24–32. https://doi.org/10.1016/S1369-7021(07)70242-0.

[2] Y. Tokura, Y. Tomioka, Colossal magnetoresistive manganites, 200 (1999) 1–23.

[3] J. Renard, CMR manganites : physics , thin films and, 127 (2003).

[4] Y. Tokura, Colossal Magnetoresistive Oxides _ Yoshinori Tokura _ Taylor & Francis, 1st Editio, CRC Press, London, 2000. https://doi.org/https://doi.org/10.1201/9781482287493.
[5] S.S.. Parkin, N. More, K.P. Roche, Oscillations in Exchange Coupling and Magnetoresistance in Metallic Superlattice Structures: Co/Ru, Co/Cr, and Fe/Cr, Phys. Rev. Lett. 64 (1990) 2304–2308. https://doi.org/DOI: https://doi.org/10.1103/PhysRevLett.64.2304.
[6] P.M. Levy, Giant Magnetoresistance in Magnetic Layered and Granular Materials*, Solid State Phys. 47 (1994) 367–472. https://doi.org/https://doi.org/10.1016/S0081-1947(08)60642-6.
[7] J.Q. Xiao, J. Samuel, Jiang, C.L. Chien, Giant Magnetoresistance in Nonmnltilayer Magnetic Systems, Phys. Rev. Lett. 68 (1992) 3749–3752.
[8] A.E. Berkowitz, J. Mitchell, R., M. Carey, J., A. Young, P., S. Zhang, F.E. Spada, F.T. Parker, A. Hutten, G. Thomas, Giant Magnetoresistance in Heterogeneous Cu-Co Alloys, Phys. Rev. Lett. 68 (1992) 3745–3748.
[9] J.K.H.A. T. L. Hylton, K. R. Coffey, M. A. Parker, Giant Magnetoresistance at Low Fields in Discontinuous NiFe-Ag Multilayer Thin Films, Science (80-.). 261 (1993) 1021–24.
[10] S. Athanasopoulos, S.W. Bailey, J. Ferrer, V.M. Garc, Giant magnetoresistance of nickel-contacted carbon nanotubes, J. Phys. Condens. Matter. 19 (2007) 042201. https://doi.org/10.1088/0953-8984/19/4/042201.
[11] I.H. KARAHAN, ¨O F BAKKALO˘GLU, M. BEDIR, Giant magnetoresistance of electrodeposited Cu – Co – Ni alloy films, Pramana. 68 (2007) 83–90.
[12] G.H.J. R, J.H.V. an Santen, FERROMAGNETIC COMPOUNDS OF MANGANESE WITH PEROVSKITE STRUCTURE, Physica. XVI (1950) 337--349.
[13] G.H. JONKER, Magnetic compounds with Perovskite Structure IV, Physica. XXII (1956) 707–722.
[14] G.C. Milward, M.J. Calderon, P.B. Littlewood, Electronically soft phases in manganites, Nature. 433 (2005) 607.
[15] M.B. Salamon, M. Jaime, The physics of manganites : Structure and transport, Rev. Mod. Phys. 73 (2001) 583–628.
[16] C.W. SEARL, S.T. Wang, Studies of the ionic ferromagnet (LaPb)MnO,. V. Electric transport and ferromagnetic properties, Can. J. Phys. 28 (1970) 2023–31.
[17] C.W. Searl, S.T. Wang, Studies of the ionic ferromagnet (LaPb)MnO,. III. Ferromagnetic resonance studies, Can. J. Phys. 47 (1969) 2703–2708.
[18] C. Israel, M.J. Calderón, N.D. Mathur, The current spin on manganites, Mater. Today. 10 (2007) 24–32.
[19] A. M. GLAZER, Simple Ways of Determining Perovskite Structures, Acta Crystallogr. A31 (1975) 756–762.
[20] von V.M. Goldschmidt., Geochemische Verteilungsgesetze der Elemente in SearchWorks catalog, (n.d.) 8v.
[21] C.N.R. Rao, A.K. Raychaudhurit, COLOSSAL MAGNETORESISTANCE , CHARGE ORDERING AND OTHER NOVEL PROPERTIES OF MANGANATES AND RELATED MATERIALS, 1998. https://doi.org/https://www.worldscientific.com/doi/abs/10.1142/9789812816795_0001.
[22] E.O. Wollan, W.C. Koehler, Neutron Diffraction Study of the Magnetic Properties of the Series of Perovskite-Type Compounds L(1—x)La, xCa]MnO3, Phys. Rev. 100 (1955) 1955.
[23] L.K. Leung, A.H. Morrish, C.W. Searle, Studies of the ionic ferromagnet (LaPb)MnO,. II. Static magnetization properties from 0 to 800 0K, Can. J. Phys. 47 (1969) 2697.
[24] J.. Jirák, Z., Vratislav, S. and Zajiček, The Magnetic Structure of Pr0.9 Ca 0.1 MnO 3, 42 (1979) 411–417. https://doi.org/doi.org/10.1515/9783112496862-051.
[25] John B Goodenough, Theory of the Role of Covalence in the Perovskite-Type Manganites [La,M(II)]MnO3, Phys. Rev. 100 (1955) 564.
[26] J.M.D. Coey, M. Viret, S. Von Molnár, Mixed-valence manganites, Adv. Phys. 58 (2009) 571–697. https://doi.org/10.1080/00018730903363184.
[27] C. Zener, Interaction between the d-Shells in the Transition Metals. II. Ferromagnetic Comyountls of Manganese with Perovskite Structure, Phys. Rev. 82 (1950).
[28] A. V. Deshmukh, S.I. Patil, S.M. Bhagat, P.R. Sagdeo, R.J. Choudhary, D.M. Phase, Effect of iron doping on electrical, electronic and magnetic properties of La0.7Sr0.3MnO3, J. Phys. D. Appl. Phys. 42 (2009) 1–6. https://doi.org/10.1088/0022-3727/42/18/185410.
[29] B. D. Cullity, C. D. Graham, Introduction to Magnetic Materials, IEEE Press, A John Wiley and sons, INC., Publication, 2009.
[30] G. Channagoudra, A.K. Saw, V. Dayal, Low temperature spin polarized tunnelling magneto-resistance in La1-xCaxMnO3 (x=0.375 and 0.625) nanoparticles, Emergent Mater. 3 (2020) 45–49. https://doi.org/10.1007/s42247-019-00067-z.
[31] V. Dayal, S. Keshri, Structural and magnetic properties of La0.67Ca0.33Mn(1-x)FexO3 (x=0-0.07), Solid State Commun. 142 (2007). https://doi.org/10.1016/j.ssc.2007.01.022.

[32] C. Zener, Interaction between the d-shells in the transition metals. II. Ferromagnetic compounds of manganese with Perovskite structure, Phys. Rev. 82 (1951) 403–405. https://doi.org/10.1103/PhysRev.82.403.
[33] P.W. Anderson, H. Hasegawa, Considerations on double exchange, Phys. Rev. 100 (1955) 675–681. https://doi.org/10.1103/PhysRev.100.675.
[34] P. Kameli, H. Salamati, A. Aezami, Influence of grain size on magnetic and transport properties of polycrystalline La0.8Sr0.2MnO3 manganites, J. Alloys Compd. 450 (2008) 7–11. https://doi.org/10.1016/j.jallcom.2006.10.078.
[35] N.D. Thorat, K.P. Shinde, S.H. Pawar, K.C. Barick, C.A. Betty, R.S. Ningthoujam, Polyvinyl alcohol: An efficient fuel for synthesis of superparamagnetic LSMO nanoparticles for biomedical application, Dalt. Trans. 41 (2012) 3060–3071. https://doi.org/10.1039/c2dt11835a.
[36] M.E. Botello-Zubiate, M.C. Grijalva-Castillo, D. Soto-Parra, R.J. Sáenz-Hernández, C.R. Santillán-Rodríguez, J.A. Matutes-Aquino, Preparation of La 0.7 Ca 0.3-x Sr x MnO 3 manganites by four synthesis methods and their influence on the magnetic properties and relative cooling power, Materials (Basel). 12 (2019). https://doi.org/10.3390/ma12020309.
[37] K. Navin, R. Kurchania, A comparative study of the structural, magnetic transport and electrochemical properties of La0.7Sr0.3MnO3 synthesized by different chemical routes, Appl. Phys. A Mater. Sci. Process. 126 (2020) 1–13. https://doi.org/10.1007/s00339-019-3269-2.
[38] H.M. Rietveld, A profile refinement method for nuclear and magnetic structures, J. Appl. Crystallogr. 2 (1969) 65–71. https://doi.org/10.1107/s0021889869006558.
[39] H.M. Rietveld, The Rietveld method, Phys. Scr. 89 (2014). https://doi.org/10.1088/0031-8949/89/9/098002.
[40] J. Rodríguez-Carvajal, Recent advances in magnetic structure determination by neutron powder diffraction, Phys. B Phys. Condens. Matter. 192 (1993) 55–69. https://doi.org/10.1016/0921-4526(93)90108-I.
[41] A. L. Patterson, The Scherrer Formula for X-Ray Particle Size Determination, Phys. Rev. 56 (1938) 978.
[42] S.O. Manjunatha, A. Rao, T.Y. Lin, C.M. Chang, Y.K. Kuo, Effect of Ba substitution on structural, electrical and thermal properties of La0.65Ca0.35-xBaxMnO3($0 \leq x \leq 0.25$) manganites, J. Alloys Compd. 619 (2015) 303–310.ttps://doi.org/10.1016/j.jallcom.2014.09.042.
[43] S.P. Rao, A.K. Saw, C. Chotia, G. Okram, V. Dayal, Structural and thermoelectric properties of Mn15Si26, Mn4Si7 and MnSi2, synthesized using arc-melting method, Appl. Phys. A Mater. Sci. Process. 127 (2021) 1–6. https://doi.org/10.1007/s00339-021-04754-9.
[44] C.J. Benedict, A. Rao, G. Sanjeev, G.S. Okram, P.D. Babu, A systematic study on the effect of electron beam irradiation on structural, electrical, thermo-electric power and magnetic property of LaCoO3, J. Magn. Magn. Mater. 397 (2016) 145–151. https://doi.org/10.1016/j.jmmm.2015.08.111.
[45] A.K. Saw, G. Channagoudra, S. Hunagund, F. Hao, R.L. Hadimani, V. Dayal, Study of magnetotransport and low temperature anomaly in half doped lanthanum calcium manganite nanoparticle, (2019) 030437. https://doi.org/10.1063/1.5113276.
[46] S. Keshri, V. Dayal, Structural and electrical transport properties of nanosized La0.67Ca0.33MnO3 sample synthesized by a simple low-cost novel route synthesized by a simple low-cost novel route, 70 (2008) 697–704.
[47] G. Channagoudra, S. Gupta, V. Dayal, Study of structural, transport and magneto-crystalline anisotropy in La<inf>1-x</inf>Sr<inf>x</inf>MnO<inf>3</inf>($0.30 \leq x \leq 0.40$) perovskite manganites, AIP Adv. 11 (2021). https://doi.org/10.1063/9.0000119.
[48] G. Channagoudra, S. Gupta, V. Dayal, Study of structural, transport and magneto-crystalline anisotropy in La1−xSrxMnO3 ($0.30 \leq x \leq 0.40$) perovskite manganites, AIP Adv. 11 (2021) 1–6. https://doi.org/10.1063/9.0000119.
[49] S. Keshri, V. Dayal, L. Joshi, Influence of Fe doping on electrical properties of LCMO, Phase Transitions. 81 (2008). https://doi.org/10.1080/01411590701448772.
[50] R.K. Pathria, P.D. Beale, Phase transitions_ criticality, universality, and scaling, in: Stat. Mech. (Fourth Ed., Academic Press (ScienceDirect), 2022: pp. 417–486. https://doi.org/https://doi.org/10.1016/C2017-0-01713-5.
[51] P.A.P. V.S. Zakhvalinskii, R. Laiho, A.V. Lashkul, K.G. Lisunov , E.L¨ahderanta, Yu.S. Nekrasova, Phase separation , ferromagnetism and magnetic irreversibility La1-xSrxMn1-yFeyO3, J. Magn. Magn. Mater. 323 (2011) 2186–2191. https://doi.org/10.1016/j.jmmm.2011.03.028.
[52] H.Y. Hwang, S.-W. Cheong, P.G. Radaelli, M. Marezio, B. Batlogg, Lattice Effects on the Magnetoresistance in Doped LaMn03, Phys. Rev. Lett. 75 (1995) 3–6.